



Stern- und
Planetенentstehung
Sommersemester 2020
Markus Röllig

Lecture 7: Star Formation Rate at Galactic Scales



http://exp-astro.physik.uni-frankfurt.de/star_formation/index.php

VORLESUNG/LECTURE

Raum: Physik - 02.201a

dienstags, 12:00 - 14:00 Uhr

SPRECHSTUNDE:

Raum: GSC, 1/34, Tel.: 47433, (roellig@ph1.uni-koeln.de)

dienstags: 14:00-16:00 Uhr

Nr.	Thema	Termin
1	Observing the cold ISM	21.04.2020
2	Observing Young Stars	28.04.2020
3	Gas Flows and Turbulence Magnetic Fields and Magnetized Turbulence	05.05.2020
4	Gravitational Instability and Collapse	12.05.2020
5	Stellar Feedback	19.05.2020
6	Giant Molecular Clouds	26.05.2020
7	Star Formation Rate at Galactic Scales	02.06.2020
8	Stellar Clustering	09.06.2020
9	Initial Mass Function – Observations and Theory	16.06.2020
10	Massive Star Formation	23.06.2020
11	Protostellar disks and outflows – observations and theory	30.06.2020
12	Protostar Formation and Evolution	07.07.2020
13	Late Stage stars and disks – planet formation	14.07.2020

7 STAR FORMATION RATE AT GALACTIC SCALES

7.1 OBSERVATIONS

7.1.1 The Star Formation Rate integrated over whole Galaxies

7.1.1.1 Methodology

Kennicutt (1998) & Schmidt (1959) 'discovered' a scaling between a galaxies gas density and its star formation rate

We are interested in a correlation between neutral gas and star formation rate averaged over an entire galaxy.

- gas content
 - neutral hydrogen => 21 cm line emission HI *neutral*
(weak line at low frequency => no data at high redshift!)
 - molecular gas => proxy observations H_2 *difficult to directly detect*
 - CO J=2-1 or J=1-0
 - conversion to H_2 via X-factor $^{12}\text{CO} \rightarrow \text{H}_2$
- star formation rate => proxy
- rotation rate of galaxies

7.1.1.2 Nearby Galaxies

Star formation rate vs. total gas mass shows a strong correlation

the bigger \Rightarrow the bigger

(larger galaxies show more SF and have more gas)

⇒ normalizing per (projected) galaxy surface (requires that galaxies are (marginally resolved)

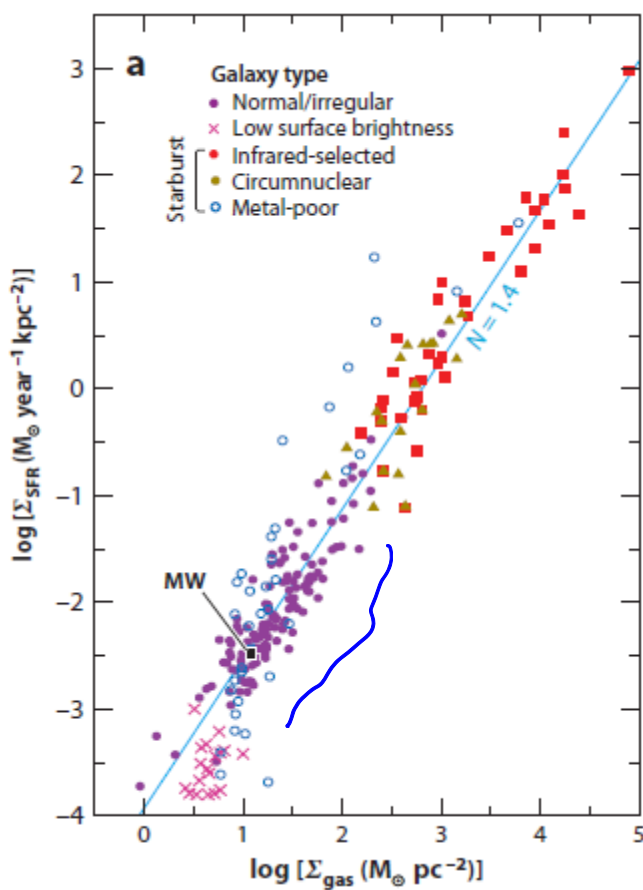


Abbildung 1 Correlation between gas surface density Σ_{gas} and star formation surface density Σ_{SFR} , integrating over whole galaxies. Galaxy classes are indicated in the legend (Kennicutt & Evans 2012)

⇒ gas mass per unit area

Σ_{gas}

⇒ star formation rate per unit area Σ_{SFR}

local galaxies:

$$\Sigma_{\text{SFR}} \propto \Sigma_{\text{gas}}^{1.4}$$

(slope may vary depending on SFR assumptions, X_{CO} scaling, etc.)

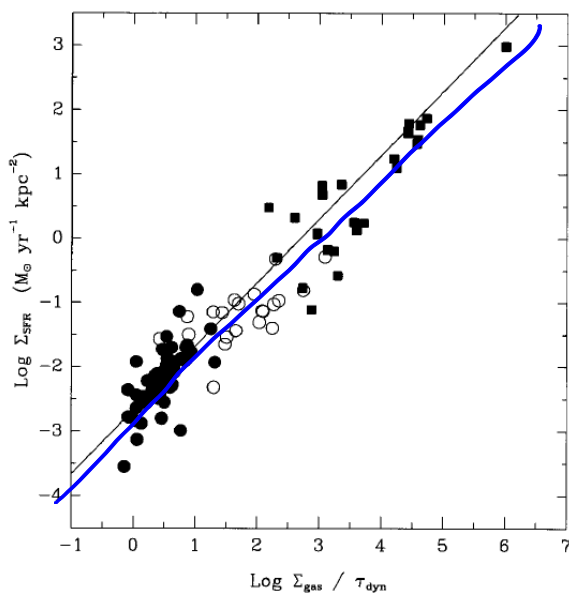


FIG. 7.—Relation between the SFR for the normal disk and starburst samples and the ratio of the gas density to the disk orbital timescale, as described in the text. The symbols are the same as in Fig. 6. The line is a median fit to the normal disk sample, with the slope fixed at unity as predicted by equation (7).

Abbildung 2 Kennicutt (1998)

use of rotation curve:

$$\Sigma_{\text{gas}}/\tau_{\text{dyn}}$$

has units of $\text{kg s}^{-1} \text{cm}^{-2}$

similar to $[\Sigma_{\text{SFR}}] = \text{kg s}^{-1} \text{cm}^{-2}$

relation describes what fraction of gas is converted into stars per orbital period

7.1.1.3 High Redshift Galaxies

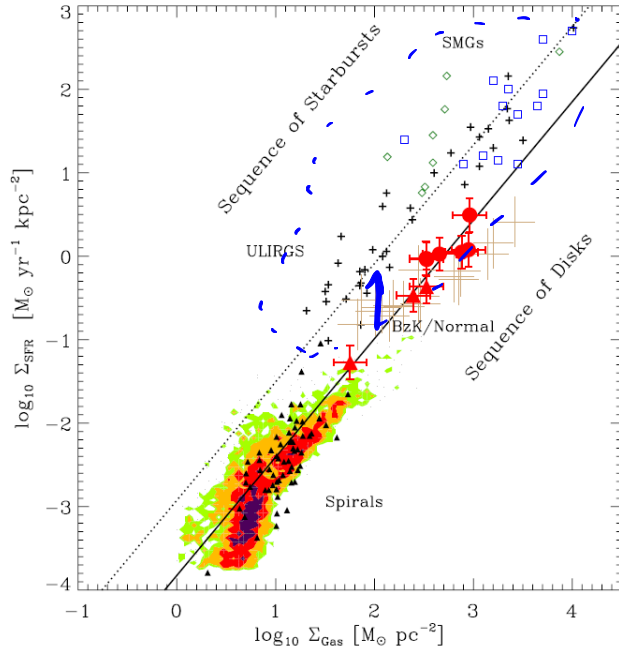


Abbildung 3 Daddi et al. 2010

Figure 2. SFR density as a function of the gas (atomic and molecular) surface density. Red filled circles and triangles are the BzKs (D10; filled) and $z \sim 0.5$ disks (F. Salmi et al. 2010, in preparation), brown crosses are $z = 1\text{--}2.3$ normal galaxies (Tacconi et al. 2010). The empty squares are SMGs: Bouché et al. (2007; blue) and Bothwell et al. (2009; light green). Crosses and filled triangles are (U)LIRGs and spiral galaxies from the sample of K98. The shaded regions are THINGS spirals from Bigiel et al. (2008). The lower solid line is a fit to local spirals and $z = 1.5$ BzK galaxies (Equation (2), slope of 1.42), and the upper dotted line is the same relation shifted up by 0.9 dex to fit local (U)LIRGs and SMGs. SFRs are derived from IR luminosities for the case of a Chabrier (2003) IMF.

adding high z data suggests no single relationship but

- ⇒ normal galaxies
- ⇒ starburst galaxies

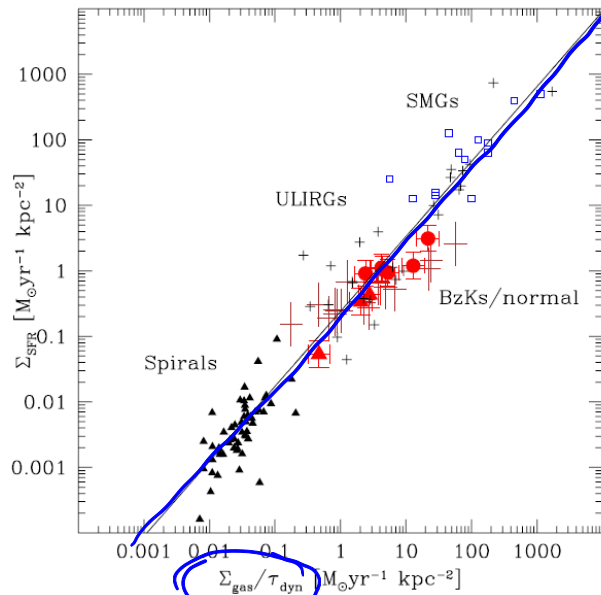


Abbildung 4 Daddi et al. 2010

but normalizing to dynamical time scale still yields a strong correlation.

7.1.1.4 Dwarfs and low surface brightness galaxies

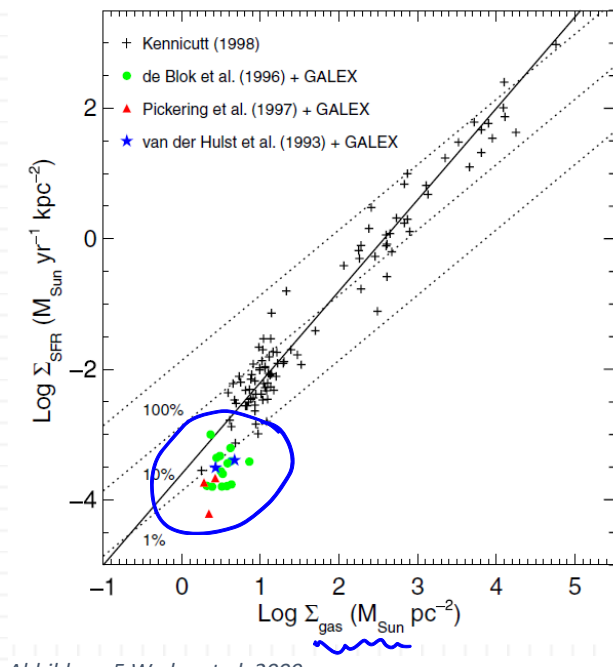


Figure 17. SFR surface density as a function of the total hydrogen gas surface density. The colored symbols indicate the sample of 19 LSB galaxies from this paper with SFRs measured from the UV with no correction for dust attenuation. The gas surface densities are derived from the H I data from de Blok et al. (1996) (green circles), Pickering et al. (1997) (red triangles), and van der Hulst et al. (1993) (blue stars) and assume that the molecular fraction is negligible. The black pluses indicate the sample of higher surface brightness galaxies from Kennicutt (1998a) while the solid line is the power-law fit to these points with exponent 1.4. The dotted lines indicate lines of constant star formation efficiency assuming a star formation time scale of 10^8 yr. The LSB galaxies tend to lie below the extrapolation of the power-law fit to the higher surface brightness sample.

Only after GALEX (FUV) and Herschel (FIR) data was available this could be measured because dwarfs are too faint in H α and the X $_{CO}$ factor is definitely different.



Dwarfs fall below the Kennicutt-Schmidt law!

7.1.2 The Spatially-Resolved Star Formation Rate

Thanks to technological advances!

7.1.2.1 Relationship to Molecular Gas

@ 0.5-1 kpc => very good correlation between molecular gas and SFR

in inner disks of nearby galaxies (CO detectable) we find a roughly constant depletion time

$$t_{dep} = \frac{\Sigma_{H_2}}{\Sigma_{SFR}} \approx 2 \text{ Gyr}$$

basically, insensitive to any other property of the galaxy, e.g. orbital time scale!

Surprising since normalizing to t_{dyn} reduced scatter Kennicutt-Schmidt law.

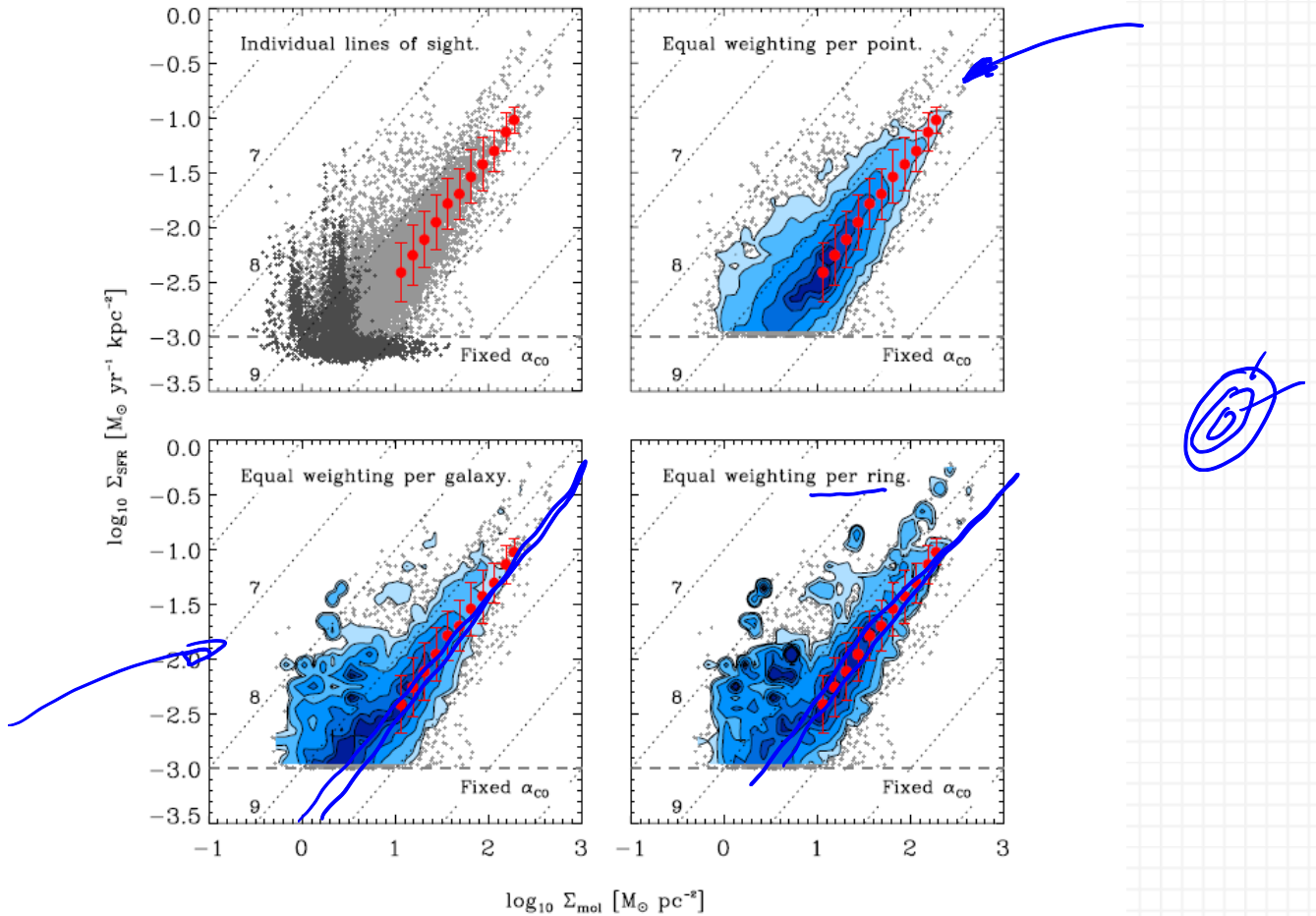
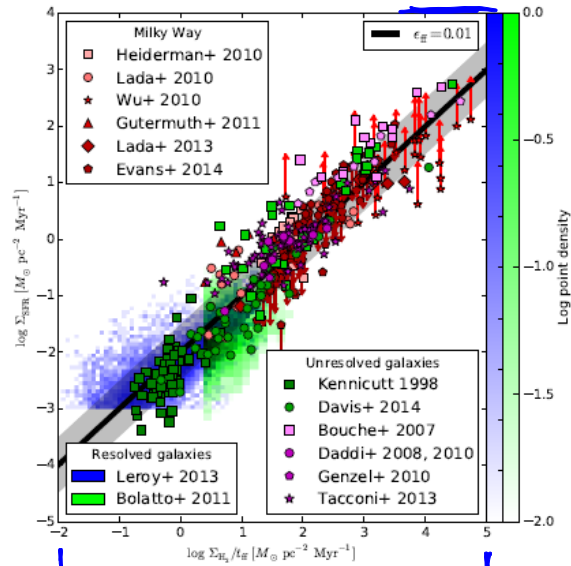


Figure 1. Star formation rate surface density, Σ_{SFR} , estimated from $\text{H}\alpha+24\mu\text{m}$ emission, as a function of molecular gas surface density, Σ_{mol} , derived from CO (2–1) emission for 30 nearby disk galaxies. The top left panel shows individual points (dark gray points show upper limits) with the running median and standard deviation indicated by red points and error bars. The red points with error bars from the first panel appear in all four panels to allow easy comparison. Dotted lines indicated fixed H_2 depletion times; the number indicates $\log_{10} \tau_{\text{Dep}}$ in yr. The top right panel shows the density of the data in the top left panel. In the bottom panels we vary the weighting used to derive data density. The bottom left panel gives equal weight to each galaxy. The bottom right panel gives equal weight to each galaxy and each radial bin.

Abbildung 6 Leroy et al. 2013



(Krumholz 2014)

normalizing K-S law by t_{ff}

(difficult to determine!)

Figure 4: Surface density of star formation versus surface density of molecular gas normalized by estimated free-fall time Σ/t_{ff} . The free-fall time for all objects has been estimated following the method of Krumholz et al. (2012a). The black thick line shows $e_{ff} = 0.01$; the gray band indicates a factor of 3 scatter about this value. The data shown in the plot are as follows: individual molecular clouds in the Milky Way (red-hued points) are from Heiderman et al. (2010, red squares), Lada et al. (2010, red circles), Wu et al. (2010, red stars, upward arrows indicate lower limits), Lada et al. (2013, red diamonds), and Evans et al. (2014, red pentagons; downward arrows indicate upper limits); resolved observations of nearby galaxies (rasters, same data as shown in Figure 3) are from a sample of the inner disks of spirals (Leroy et al. 2013, blue raster) and the 12 pc resolution data form the Small Magellanic Cloud (Bolatto et al. 2011, green raster); unresolved observations of $z = 0$ galaxies (green points) are spirals and starbursts from Kennicutt (1998a, green squares), and the molecular disks of early-type galaxies from Davis et al. (2014); unresolved observations of $z > 0$ galaxies (magenta points) are from Bouche et al. (2007, magenta squares), Daddi et al. (2008, 2010b, magenta circles), Genzel et al. (2010, magenta pentagons), and Tacconi et al. (2013, magenta stars). All CO-to- H_2 conversion factors have been standardized to the fiducial values of Daddi et al. (2010a): $\alpha_{\text{CO}} = 0.8 M_{\odot}/(\text{K km s}^{-1} \text{ pc}^{-2})$ in starbursts at all redshifts, $\alpha_{\text{CO}} = 4.6 M_{\odot}/(\text{K km s}^{-1} \text{ pc}^{-2})$ in $z = 0$ disks, and $\alpha_{\text{CO}} = 3.6 M_{\odot}/(\text{K km s}^{-1} \text{ pc}^{-2})$ in $z > 0$ disks. Within each data set, lighter colored points are those for which a starburst-like α_{CO} value was adopted, while darker points are those using a disk-like α_{CO} . The exception is the early-type galaxy sample of Davis et al. (2014), where it is not clear which to use, and I have therefore deferred to their recommended, intermediate value $\alpha_{\text{CO}} = 3.4 M_{\odot}/(\text{K km s}^{-1} \text{ pc}^{-2})$.

Caveats:

- ⇒ limited to inner parts of galaxies with significant CO
- ⇒ limited galaxy sample $D \lesssim 20$ Mpc (no starbursts in this volume)
- ⇒ correlation strength depends on scales over which we average
 - on sufficiently small scales we do not look at an average piece of galaxy any more
 - proxies carry different information
 - CO: momentaneous mol. gas content
 - H α : average # of stars formed in the last ~5Myr
 - relating each other is misleading
 - on larger scales this averages out

7.1.2.2 Relationship to Atomic Gas

Very different results for total (or atomic) gas.

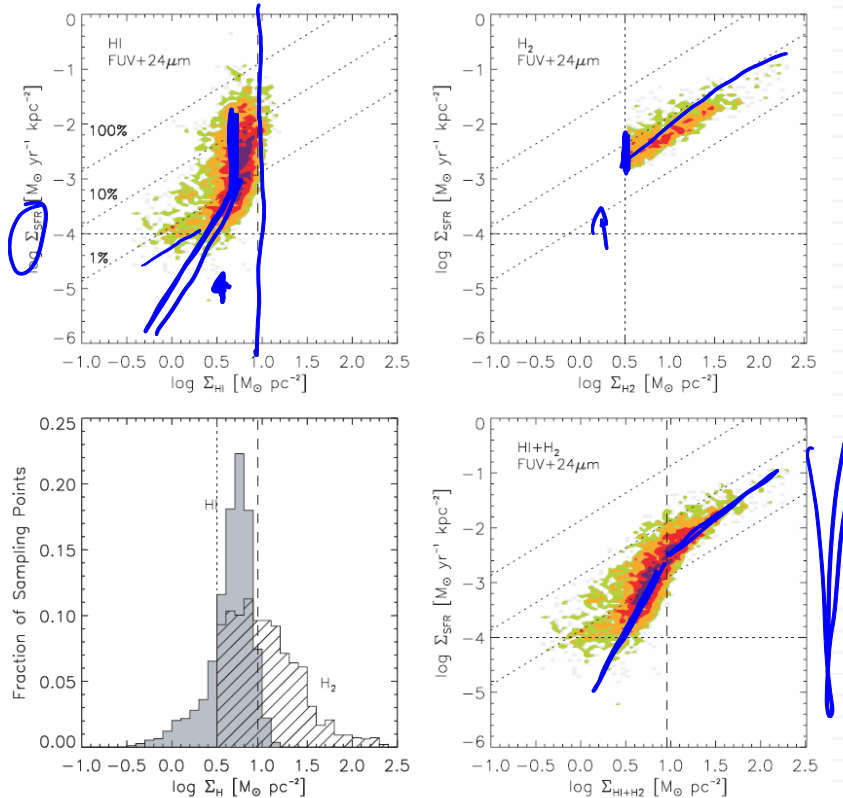


Abbildung 7 K-S law for HI gas in inner galaxies, averaged for ~ 750 pc scales (Bigiel et al. 2009)

HI surface density reaches a maximum is uncorrelated to SFR @ this max.

In inner parts of galaxies, SF does not care about atomic gas

In contrast to that: in the outer parts of galaxies there seems to be a correlation to the HI gas

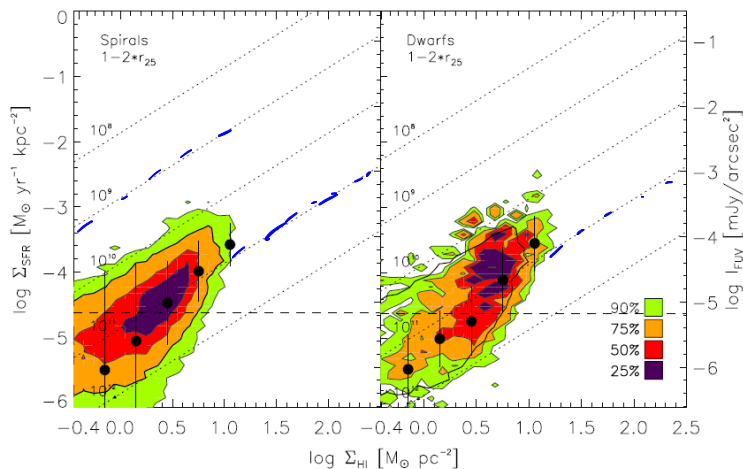


Abbildung 8 Bigiel et al. 2010, K-S-law for HI gas in outer galaxies on ~ 750 pc scales.

here very long

$t_{dep} \sim 100$ Gyr

probably result of very low
H₂-HI ratio of 1-2%

because if CO is detectable
we still find

$t_{dep,mol\ gas} \sim 2$ Gyr

When plotting SFR against mol. + atomic gas we find a clear correlation

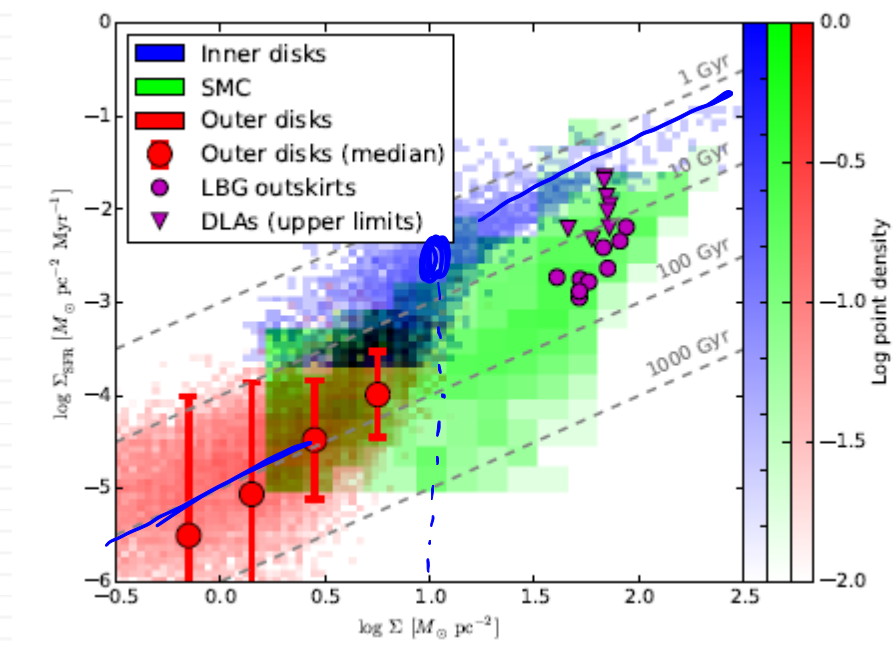


Abbildung 9 Krumholz 2014

@ high Σ

most gas is in H₂

$t_{dep} \sim 2$ Gyr

@ low Σ

most gas is in HI

$t_{dep} \sim 100$ Gyr

SFR drops by factor
of 50

7.1.3 Star Formation in dense gas

7.1.3.1 Alternatives to CO

So far: CO as H₂ proxy

Next brightest mol. line in galaxies: HCN (HCO⁺, CS, and HNC)

~10 times fainter than CO (100 x mapping times!)

Comparison:

- Energy levels
 - CO: 5.5, 16.6, 33.3, 55.4 K
 - HCN: 4.3, 12.8, 25.6, 42.7 K
- Coll. de-excitation rates for 1-0
 - CO: $k_{10} = 3.3 \times 10^{-11} \text{ cm}^3 \text{s}^{-1}$
 - HCN: $k_{10} = 2.4 \times 10^{-11} \text{ cm}^3 \text{s}^{-1}$
- Einstein A-values for 1-0
 - CO: $A_{10} = 7.2 \times 10^{-8} \text{ s}^{-1}$
 - HCN: $A_{10} = 2.4 \times 10^{-5} \text{ s}^{-1}$
- critical density for 1-0
 - CO: $n_{crit} = 2200 \text{ cm}^{-3}$
 - HCN: $n_{crit} = 10^6 \text{ cm}^{-3}$

HCN => tracer of dense gas!

Correlation with SFR but somewhat lower slope than with CO!

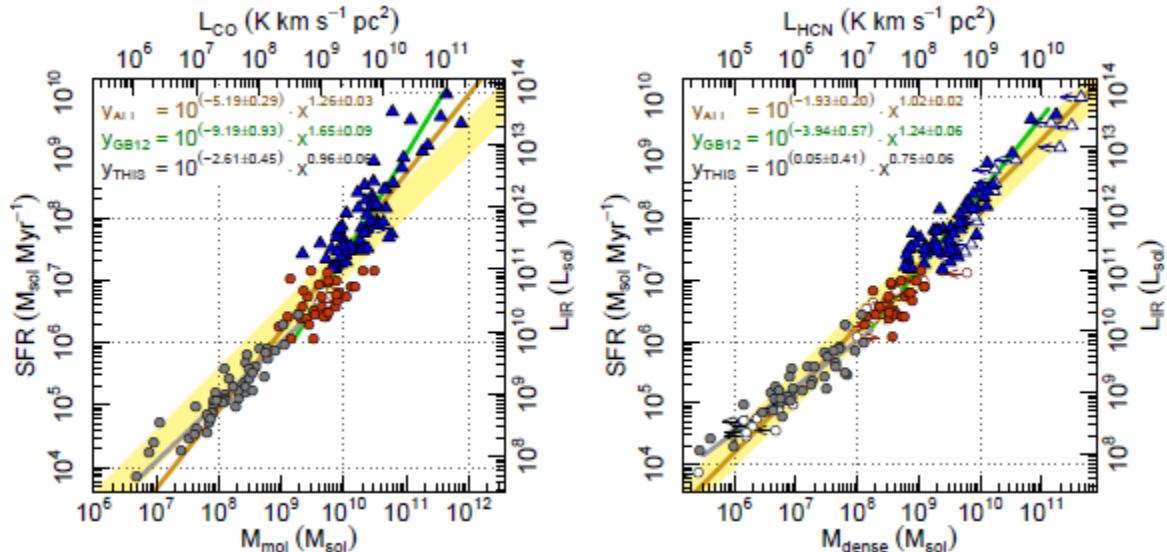


Figure 1. Top row: Total SFR (Σ_{SFR}) as a function of the mass of molecular (left) and dense (right) molecular gas for pointings in galaxy disks (this paper, gray points) and unresolved star-forming galaxies (red) and (U)LIRGs (blue) from GB12. Bottom row: Surface density of recent SFR (Σ_{SFR}) as a function of the surface density of total (left) and dense (right) molecular gas for the same data sets. The top and right-hand axes of each panel display the data in terms of observed quantities. Open symbols indicate limits in the direction of the attached arrows. The equations in the figures report power-law fits to our data (gray line), the GB12 sample (green line), and all the data (brown line). Errors at 1σ -level in the fit parameters are indicated. For comparison, the yellow area shows a fixed ratio (power law index 1) with a factor of 2 scatter.

Abbildung 10 Usero et al. 2015

7.2 THEORY

Any successful theory needs to reproduce the main observational results:

- SF appears to be very slow or inefficient $t_{dep} \approx 100 \times t_{ff}$
- in unresolved observations, the SFR rises non-linearly with total gas content
- in central disks of galaxies SF correlates strongly with molecular gas and poorly with atomic gas
- constant t_{dep} in nearby normal galaxies, shorter t_{dep} in actively star-forming galaxies
- A correlation between SF and atomic gas only where the gas content is dominated by atomic phase. Then
 $t_{dep,mol.} \approx 100 \times t_{dep,atom}$
- If dense gas tracers are used t_{dep} is shorter than for the bulk of the molecular gas, but still much longer than t_{ff}

At present, no theory explains all the observations!

- top-down model: SF regulated by galactic-scale processes
- bottom-up model: SF regulated within molecular clouds

7.2.1 The Top-Down approach

7.2.1.1 Hydrodynamics plus Gravity

Simplest ansatz: only hydrodynamics & gravity, no feedback

- ⇒ baseline models
- ⇒ study of large-scale gravitational instability

$$Q = \frac{\Omega\sigma}{\pi G\Sigma} \quad \text{Toomre (1964) Q parameter}$$

Ω : angular velocity of disk rotation, σ : gas velocity dispersion, Σ : gas surface density

- $Q < 1$ system unstable to axi-symmetric perturbations
- $Q > 1$ system stable

Observed galactic disks $Q \approx 1$ for majority of disk and $Q > 1$ at edges
stable



If $Q \approx 1$: grav. instability (self-gravity of disk) occurring on galactic scale might be an important driver of star formation.

If $Q > 1$: grav. instability unimportant on large scales, SF occurs locally, where global structures (e.g. spiral waves) compress the gas.

- Usually these models give $\epsilon_{ff} \sim 1$ (rather than 0.01) because nothing stops a collapse once it begins.
- No dependence on metallicity (which is observed)

7.2.1.2 Feedback Regulated Models

Gas-momentum equation without viscosity and with magnetic fields:

$$\frac{\partial}{\partial t}(\rho \vec{v}) = -\nabla \cdot (\rho \vec{v} \vec{v}) - \nabla P + \frac{1}{4\pi} \nabla \cdot \left(\vec{B} \vec{B} - \frac{B^2}{2} \vec{I} \right) + \rho \vec{g}$$

disk in x-y plane. Only take z-component:

$$\frac{\partial}{\partial t}(\rho v_z) = -\nabla \cdot (\rho \vec{v} v_z) - \frac{dP}{dz} + \frac{1}{4\pi} \nabla \cdot (\vec{B} B_z) - \frac{1}{8\pi} \frac{d}{dz} B^2 + \rho g_z$$

Consider some area A at constant height z , average over A :

$$\begin{aligned} \frac{\partial}{\partial t} \langle \rho v_z \rangle &= -\frac{1}{A} \int_A \nabla \cdot (\rho \vec{v} v_z) dA - \frac{d\langle P \rangle}{dz} + \frac{1}{4\pi A} \int_A \nabla \cdot (\vec{B} B_z) dA \\ &\quad - \frac{1}{8\pi} \frac{d}{dz} \langle B^2 \rangle + \langle \rho g_z \rangle \end{aligned}$$

$\langle Q \rangle = \frac{1}{A} \int_A Q dA$

separate xy components from z component in divergences (and apply divergence theorem)

$$\begin{aligned} \frac{\partial}{\partial t} \langle \rho v_z \rangle &= -\frac{d\langle P \rangle}{dz} - \frac{1}{8\pi} \frac{d}{dz} \langle B^2 \rangle + \langle \rho g_z \rangle - \frac{d}{dz} \langle \rho v_z^2 \rangle + \frac{1}{4\pi} \frac{d}{dz} \langle B_z^2 \rangle \\ &\quad - \frac{1}{A} \int_A \nabla_{xy} \cdot (\rho \vec{v} v_z) dA + \frac{1}{4\pi A} \int_A \nabla_{xy} \cdot (\vec{B} B_z) dA \\ \boxed{\frac{\partial}{\partial t} \langle \rho v_z \rangle} &= -\frac{d\langle P \rangle}{dz} - \frac{1}{8\pi} \frac{d}{dz} \langle B^2 \rangle + \langle \rho g_z \rangle - \frac{d}{dz} \langle \rho v_z^2 \rangle + \frac{1}{4\pi} \frac{d}{dz} \langle B_z^2 \rangle \\ &\quad - \frac{1}{A} \int_{\partial A} v_z \rho \vec{v} \hat{n} d\ell + \frac{1}{A} \int_{\partial A} B_z \vec{B} \cdot \hat{n} d\ell \end{aligned}$$

∂A : boundary of A , \hat{n} : unit vector normal to boundary (always lies in xy plane)



$\frac{1}{A} \int_{\partial A} v_z \rho \vec{v} \cdot \hat{n} d\ell$: advection of momentum ρv_z across edges of the area

if galaxy with no net flow in galaxy $\rightarrow 0$

$\frac{1}{A} \int_{\partial A} B_z \vec{B} \cdot \hat{n} d\ell$: rate at which z momentum is transmitted across

boundary by magnetic stresses, again $\rightarrow 0$

galactic disk \sim time steady: $\frac{\partial}{\partial t} \rightarrow 0$

Equation of hydrostatic balance for galactic disk:

$$\frac{d}{dz} \langle P + \rho v_z^2 + \frac{1}{8\pi} B^2 \rangle - \frac{1}{4\pi} \frac{d}{dz} \langle B_z^2 \rangle - \langle \rho g_z \rangle = 0$$

$\frac{d}{dz} \langle P + \rho v_z^2 + \frac{1}{8\pi} B^2 \rangle$: upward force due to gradients in the total pressure, incl. turb. pressure ρv_z^2 and magn. pressure $B_z^2 / 4\pi$

$\langle \rho g_z \rangle$: downward force due to gravity

$\frac{1}{4\pi} \frac{d}{dz} \langle B_z^2 \rangle$: forces due to magnetic tension (usually not dominant).

\Rightarrow balancing first and last term!

force $\equiv \frac{d}{dt} p$ \equiv momentum flux

Each term: rate (per unit area) at which momentum is transported up or down.

Feedback Ansatz: rate in the first term = rate of momentum injected by feedback

$$\langle P + \rho v_z^2 + \frac{1}{8\pi} B^2 \rangle \sim \langle \frac{p}{M} \rangle \Sigma_{SFR}$$

$\langle \frac{p}{M} \rangle$: momentum yield per unit mass of stars formed (includes any feedback process we can come up with)

Gravity of an infinite slab of gas: $g_z = 2\pi G \Sigma$

$$\frac{d}{dz} \left(\langle \frac{p}{M} \rangle \Sigma_{SFR} \right) \sim 2\pi G \Sigma \Rightarrow \Sigma_{SFR} \sim 2\pi G \left(\frac{p}{M} \right)^{-1} \Sigma \Sigma_{gas}$$

assuming $\frac{d}{dz} \sim 1/h$, therefore $\rho h \sim \Sigma_{gas}$

In such a model we expect the SFR to scale with $\Sigma \Sigma_{gas}$.

If the gas dominates the gravity:

$$\Sigma_{SFR} \propto \Sigma_{gas}^2$$

If the stars dominate the gravity:

$$\Sigma_{SFR} \propto \Sigma_{gas} \Sigma_*$$

If we know $\left(\frac{p}{M} \right)$ we can compute SFR quantitatively.

Example:

total momentum yield of supernovae: $\left(\frac{p}{M} \right) \sim 3000 \text{ km s}^{-1}$

- $\Sigma_{SFR} \sim 0.09 M_\odot \text{pc}^{-2} \text{Myr}^{-1} \left(\frac{\Sigma}{100 M_\odot \text{pc}^{-2}} \right)^2$

~ right magnitude for observed SFRs

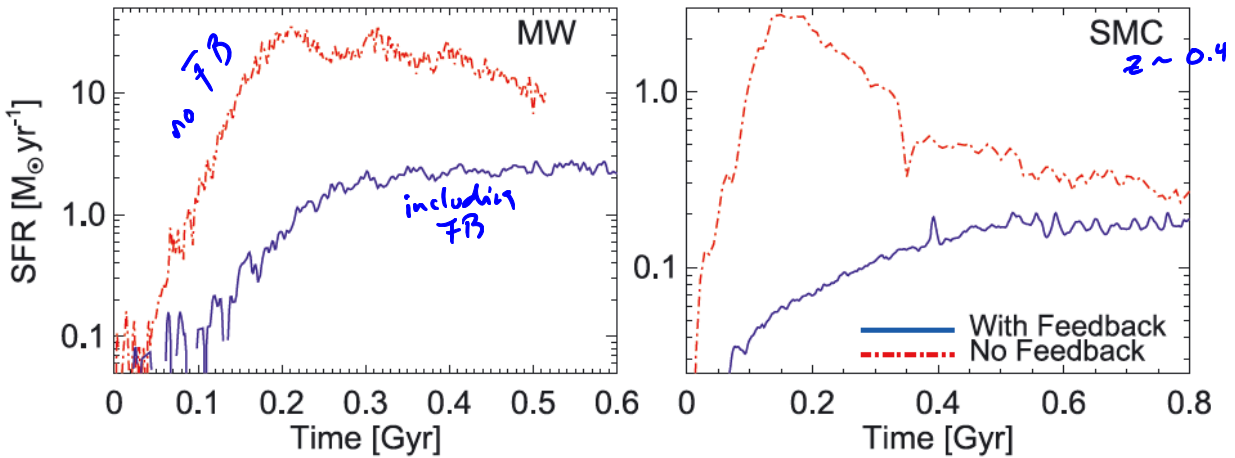
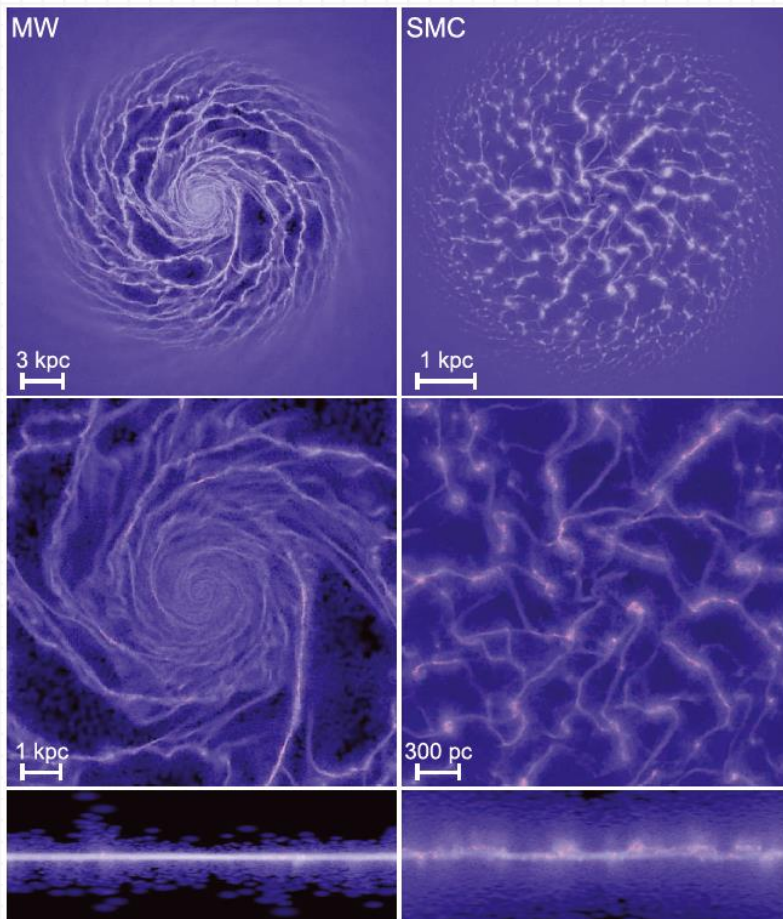


Abbildung 11 Hopkins et al. 2011: SFR versus time from simulations of isolated galaxies performed with (blue) and without (red) a subgrid mode for stellar feedback. MW (Milky Way) SMC: Small Magellanic Clouds



Successes:

- physically motivated
- allow quant.
- computation of SFR (in models and analytically)
- SFR independent of microphysics and cloud scale processes
- $\Sigma_{SFR} \propto \Sigma_{gas} \Sigma_*$ agrees with what we find in the outer MW.

Problems:

- SFR predictions depends on assumptions about $\left(\frac{p}{M}\right)$
- In the gas dominated case we expect $\Sigma_{SFR} \propto \Sigma_{gas}^2$, but we observe (Kennicutt-Schmidt relation) $\propto \Sigma_{gas}^{1.4}$ |
- Even though the SFR in the outer MW matches the model predictions, the model doesn't care about metallicity. But we observe a metallicity dependence
- The feedback approach doesn't distinguish between H and H₂

- Observations suggest that SF is equally slow in clouds and in whole galaxies. In the feedback models this is not required. We can have fast SF in clouds and slow in the whole galaxy. But, then why do we observe a slow SFR where we have no feedback (as in the solar neighborhood)?

7.2.2 The Bottom-Up Approach

Start SF from individual clouds.

- Which parts of a galaxy's ISM are eligible to form stars
- SFR within individual clouds

7.2.2.1 *Which gas is star forming?*

Observationally: stars form in molecular gas. -> Where is the mol. gas in a galaxy?

Physical explanation?

H_2 and CO are cooling more efficiently?

NO! C^+ is as good as CO in cooling and not all H_2 is associated with CO!

Instead: H_2 is associated with SFR because of shielding!

Thermal balance in the ISM:

Main heating: photo-electric heating and cosmic-ray heating.

Total heating rate per H nucleus:

$$\Gamma = (4 \times 10^{-26} \chi_{FUV} Z'_d e^{-\tau_d} + 2 \times 10^{-27} \zeta') \text{ erg s}^{-1}$$

χ_{FUV} : local FUV radiation field

Z'_d : local dust metallicity

ζ' : CR ionization rate

τ_d : dust optical depth

If CO has not yet formed -> C^+ main coolant ([CII] 158μm fine structure line, 92 K)



1500 GHz

opt. thin gas, LTE: cooling rate Λ



$$\Lambda_{\text{CII}} = k_{\text{CII-H}} \delta_C E_{\text{CII}} n_H$$

$k_{\text{CII-H}} \approx 8 \times 10^{-10} e^{-T_{\text{CII}}/T}$: excitation (by collisions) rate coefficient

$T_{\text{CII}} = 91 \text{ K}$: energy of excited state

$\delta_C \approx 1.1 \times 10^{-4} Z'_d$: carbon abundance relative to hydrogen

$E_{\text{CII}} = k_B T_{\text{CII}}$: energy of the level

n_H : hydrogen number density

From $\Gamma = \Lambda$ we find T :

$$T = -\frac{T_{\text{CII}}}{\ln \left(0.36 \chi_{\text{FUV}} e^{-\tau_d} + \frac{0.018 \zeta'}{Z'_d} \right) - \ln n_{H,2}}$$

$$n_{H,2} = \frac{n_H}{100 \text{ cm}^{-3}}$$

If FUV heating dominates:

$$T \approx \frac{91 \text{ K}}{1.0 + \underbrace{\tau_d}_{\text{FUV}} - \ln \chi_{\text{FUV}} + \ln n_{H,2}}$$

If CR heating dominates:

$$T \approx \frac{91 \text{ K}}{4.0 - \ln \zeta' / \underbrace{Z'_d}_{\text{CR}} + \ln n_{H,2}}$$

Transition at $\tau_d \sim 3$

CR dominated regime $\left(\frac{\zeta'}{Z'_d} = 1 \right) \Rightarrow T = 23 \text{ K}$ (almost as low as in the CO dominated region with $T \sim 10 \text{ K}$)

FUV dominated regime and low opt. depth $\Rightarrow T \sim 100 \text{ K}$

Jeans mass:

$$M_J = \rho \lambda_J^3 = \rho \left(\frac{\pi c_s^2}{G \rho} \right)^{3/2} = 4.8 \times 10^3 M_\odot n_H^{-1/2} T_2^{3/2}$$

$$\left(T_2 = \frac{T}{100K}\right), \text{ so } M_J \text{ will differ by } \left(\frac{93}{23}\right)^{1.5} \approx \underline{\underline{8.}}$$

\Rightarrow high τ (suppresses FUV heating) and lowers the mass that is stable against collapse (by \sim one order of magnitude)

Bottom-up models: this change in M_J as a function of τ regulates the SF

In warm regions (by FUV heating) the gas is thermally stabilized

In cold regions SF proceeds efficiently

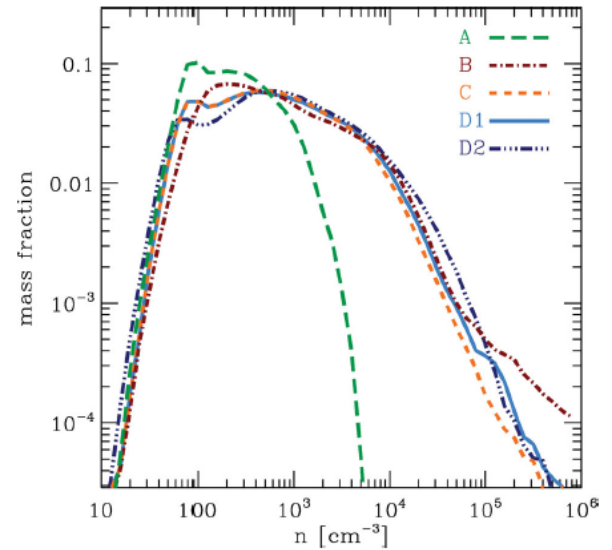
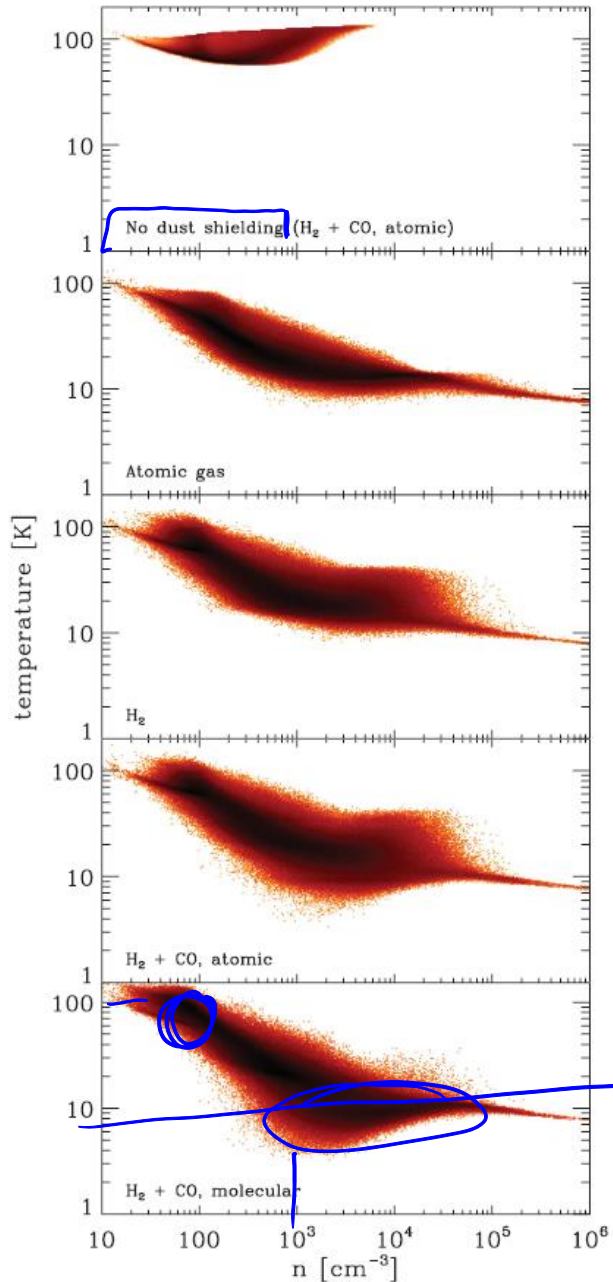


Figure 3. Comparison of the mass-weighted density PDF in the various runs. For runs B, C, D1 and D2, we show the state of the gas immediately prior to the onset of star formation, while for run A, we show the state of the gas at a similar physical time, $t = 2.3$ Myr.

Left: n - T distribution in simulations with different treatments of the ISM (Glover and Clarke 2012)

All simulations use identical initial conditions, but vary in how the gas heating and cooling rates are calculated. The top panel ignores dust shielding, but includes full chemistry and heating and cooling. The bottom panel includes all

chemistry and cooling. The middle three panels turn off, respectively, H_2 formation, CO formation, and CO cooling. The tail of material proceeding to high density in some simulations is indicative of star formation.

Relation to H₂: H₂ depends on FUV shielding

shielding column of hydrogen before H₂ can be formed:

$$N_{\text{H}} = c \frac{f_{diss} E_0^*}{n \mathcal{R}} \approx 7.5 \times 10^{20} \chi_{\text{FUV}} n_{\text{H},2}^{-1} (Z'_d)^{-1} \text{ cm}^{-2}$$

or

$$\Sigma_{\text{H}} = N_{\text{H}} \mu m_{\text{H}} = 8.4 \chi_{\text{FUV}} n_{\text{H},2}^{-1} (Z'_d)^{-1} M_{\odot} \text{ pc}^{-2}$$

This corresponds to an optical depth at which the gas becomes molecular:

$$\tau_d = N_{\text{H}} \sigma_d = 7.5 \chi_{\text{FUV}} n_{\text{H},2}^{-1} (Z'_d)^{-1}$$

($\sigma_d \approx 10^{-21} Z'_d \text{ cm}^{-2}$). About the same opt. depth at which the transition from FUV to CR dominated heating occurs.

$\chi_{\text{FUV}} n_{\text{H},2}^{-1} \sim \text{few} \times 10^{-1}$: ~const. in the MW disk because of ISM two-phase equilibrium.

- ⇒ physical explanation why SF is correlated to molecular gas
- ⇒ physical reason for breakdown at $\Sigma_{\text{H}} \leq 10 M_{\odot} \text{ pc}^{-2}$
- ⇒ metallicity dependence is also explained

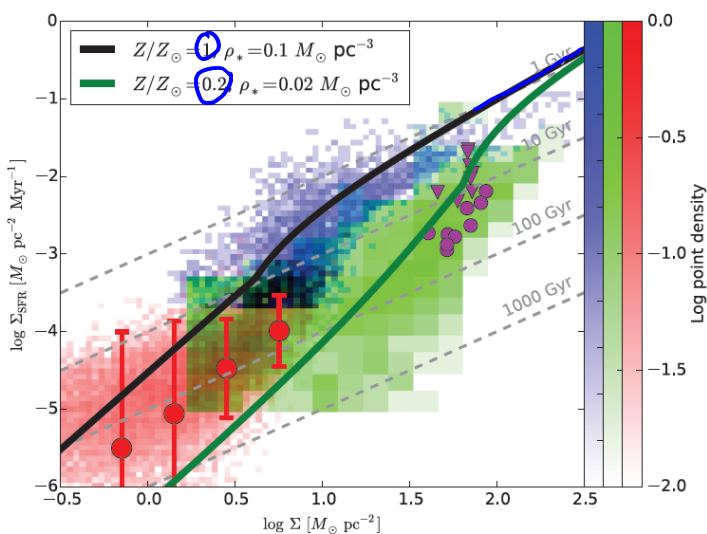


Figure 10.5: Relationship between star formation rate surface density Σ_{SFR} and total gas surface density Σ . Pixels and points show observations, and are the same as in Figure 9.11. Solid black and green lines are theoretical models from Krumholz (2013) for two different combinations of metallicity normalized to Solar, Z/Z_{\odot} , and mid-plane stellar density, ρ_{*} , as indicated in the legend.

7.2.2.2 The Star Formation Rate in Star-Forming Clouds

Overall SFR? Why is the SFR so low?

Turbulent support:

Consider a turbulent medium with linewidth-size relation

$$\sigma(l) = c_s \left(\frac{l}{\lambda_s} \right)^{1/2}$$

λ_s : sonic length. What parts of this flow will become Jeans-unstable.

The max. mass that can be held up against turbulence: Bonnor-Ebert mass:

$$M_{BE} = 1.18 \frac{c_s^3}{G^3 \rho} = \frac{1.18}{\pi^{3/2}} \rho \lambda_J^3$$

c_s : isothermal sound speed, ρ : local gas density (density at the surface of the Bonnor-Ebert sphere). The corresponding radius is:

$$\underline{R_{BE} = 0.37 \lambda_J}$$

Virial terms:

a: geometric factor
(a=0.73 max. mass sphere)

gravitational energy:

$$\mathcal{W} = -a \frac{GM_{BE}^2}{R_{BE}} = -1.06 \frac{c_s^5}{G^{3/2} \rho^{1/2}}$$

Thermal energy:

$$\mathcal{T}_{th} = \frac{3}{2} M_{BE} c_s^2 = 1.14 |\mathcal{W}|$$

Turbulent energy:

$$\mathcal{T}_{turb} = \frac{3}{2} M_{BE} \sigma (2R_{BE})^2 = 0.89 \left(\frac{\lambda_J}{\lambda_s} \right) |\mathcal{W}|$$

⇒ Collapsing parts of the flow where the density is very high

⇒ $E_{pot} \gtrsim E_{turb}$

⇒ $\lambda_J \lesssim \lambda_s$

⇒ Ansatz: Collapse if: $\lambda_J \lesssim \lambda_s$

$$\lambda_{J0} = \sqrt{\frac{\pi c_s^2}{G \bar{\rho}}} \quad \text{Jeans length at the mean density}$$

$x = \rho / \bar{\rho}$, then $\lambda_J = \lambda_{J0} / \sqrt{x}$

$$\boxed{\lambda_J \lesssim \lambda_s} \text{ then requires } x > x_{crit} \equiv \left(\phi_x \frac{\lambda_{J0}}{\lambda_s} \right)^2 \quad \phi_x \sim 1$$

mass fraction where $\lambda_J \lesssim \lambda_s$

$$f = \int_{x_{crit}}^{\infty} \frac{dp}{d \ln x} dx = \frac{1}{\sqrt{2\pi\sigma_{\rho}^2}} \int_{x_{crit}}^{\infty} \exp \left[-\frac{(\ln x - \bar{\ln x})^2}{2\sigma_{\rho}^2} \right] dx$$

$$= \frac{1}{2} \left[1 + \operatorname{erf} \left(\frac{-2 \ln x_{crit} + \sigma_{\rho}^2}{2^{3/2} \sigma_{\rho}} \right) \right]$$

$$\sigma_{\rho} \approx \left[\ln \left(1 + \frac{3M^2}{4} \right) \right]^{1/2}$$

assume a fraction f collapses every free-fall time, then the SFR per t_{ff} is

$$\epsilon_{ff} = \frac{1}{2\phi_t} \left[1 + \operatorname{erf} \left(\frac{-2 \ln x_{crit} + \sigma_{\rho}^2}{2^{3/2} \sigma_{\rho}} \right) \right] \quad \phi_t \sim 1$$

more detailed (Hennebelle & Chabrier, Federrath & Klessen):

$$\epsilon_{ff} = \frac{1}{\phi_t} \int_{x_{crit}}^{\infty} \frac{dp}{d \ln x} x^{1/2} dx$$

$$= \frac{1}{2\phi_t} \left[1 + \operatorname{erf} \left(\frac{-\ln x_{crit} + \sigma_{\rho}^2}{2^{1/2} \sigma_{\rho}} \right) \right] \exp \left(\frac{3}{8} \sigma_{\rho}^2 \right)$$

$\frac{\lambda_{J0}}{\lambda_s}$. from observations:

In regions where $\alpha_{vir} = \frac{5\sigma^2 R}{GM}$

then $\sigma(l) = \sigma_{2R} \left(\frac{l}{2R} \right)^{1/2}$ and therefore $\lambda_s = 2R \left(\frac{c_s}{\sigma_{2R}} \right)^2$

and $\lambda_{J0} = \sqrt{\frac{\pi c_s^2}{G\rho}} = 2\pi c_s \sqrt{\frac{R^3}{3GM}}$

together:
$$\underline{x_{crit}} = \left(\phi_x \frac{\lambda_{J_0}}{\lambda_s} \right)^2 = \frac{\pi^2 \phi_x^2}{15} \alpha_{vir} \mathcal{M}^2 \approx 0.82 \alpha_{vir} \mathcal{M}^2$$

For $\alpha_{vir} \approx 2$, $\epsilon_{ff} \approx 0.1$ (observed $\epsilon_{ff} \approx 0.01$) Assuming some local feedback that decreases ϵ_{ff} further puts it in the right order.

7.2.2.3 *Strengths and Weaknesses of the Bottom-Up Models*

- ⇒ B-U models reproduce SFR-ISM phase dependence
- ⇒ B-U models explain metallicity dependence
- ⇒ B-U reproduces $\epsilon_{ff} \approx 0.01$ on all scales

- ⇒ why $\epsilon_{ff} \approx 0.01$ instead of $\epsilon_{ff} \approx 0.1$ is not fully explained ✎
- ⇒ global regulation of the ISM and its hydro-balance not addressed
(where does the initial hydrostatic balance comes from?)